Transverse rectification in density-modulated two-dimensional electron gases

A. Ganczarczyk, S. Rojek, A. Quindeau, M. Geller, A. Hucht, C. Notthoff, J. König, and A. Lorke
Faculty of Physics and CENIDE, University Duisburg-Essen, Lotharstraße 1, 47057 Duisburg, Germany

D. Reuter and A. D. Wieck
Applied Solid State Physics, Ruhr-Universität Bochum, Universitätsstraße 150, 44780 Bochum, Germany
(Received 15 June 2012; published 15 August 2012)

We demonstrate tunable transverse rectification in a density-modulated two-dimensional electron gas (2DEG). The density modulation is induced by two surface gates, running in parallel along a narrow stripe of 2DEG. A transverse voltage in the direction of the density modulation is observed, i.e., perpendicular to the applied source-drain voltage. The polarity of the transverse voltage is independent of the polarity of the source-drain voltage, demonstrating rectification in the device. We find that the transverse voltage U_y depends quadratically on the applied source-drain voltage and nonmonotonically on the density modulation. The experimental results are discussed in the framework of a diffusion thermopower model.

DOI: 10.1103/PhysRevB.86.085309 PACS number(s): 73.40.Ei, 72.20.Pa

I. INTRODUCTION

One of the most striking features of mesoscopic structures is the fact that their properties are no longer solely given by the underlying material properties, but also by their size and shape. As an example, the unipolar output of a ballistic rectifier[1] is not based on a change in material (such as a Schottky contact or the doping concentration in a *p*-*n* junction) but on the introduction of a symmetry-breaking scatterer. Since this is a completely new concept for the realization of functional devices, quite a bit of work has been devoted to understanding the basic principles that lead to rectification in symmetry-broken structures,[2–7] which have been shown to operate even at elevated temperatures[2,8,9] and high frequencies.[8–11] While the original, intuitive model of ballistically guided electrons can already account for many qualitative features observed in the experiment,[1] further studies have shown that a number of different effects contribute to the observed rectification. These include quantum effects, predicted by Fleischmann *et al*.[12] and observed by de Haan *et al*.,[13] as well as thermoelectric contributions and self-gating.[14,15] Many of the investigated devices have quite elaborate designs in order to separate out a certain contribution or to optimize the rectification efficiency.

In the present work, we investigate transverse rectification in a two-dimensional electron gas (2DEG). By transverse, we mean that the unipolar voltage output is perpendicular to the applied input current. We choose a simple design, which consists of two connected, parallel 2DEG stripes of different carrier density [see Fig. 1(a)]. Thus, the broken symmetry is only induced by the modulation of the carrier density and, contrary to earlier studies, the device is featureless along the current direction. In particular, no scatterers are induced to guide or impede the flow of current. We find that the broken symmetry is sufficient to observe a clear rectification signal with a polarity that is given by the sign of the density difference. The experimental data are explained within a diffusion thermopower model that takes into account the spatial variation of the electron temperature and the thermopower. The simplicity of the sample design allows for a direct comparison between theoretical results and experimental data. We find a good quantitative agreement without any adjustable parameters.

II. EXPERIMENTAL DETAILS

The samples are fabricated from a modulation-doped GaAs/AlGaAs heterostructure grown by molecular beam epitaxy. Sample A is used for the rectification experiments, sample B is a reference sample. The samples contain a 2DEG, situated 107 nm below the surface. The charge carrier density n_0 and mobility μ_0 at $T = 4.2$ K are 2.07×10^{15} m^{-2} and 125 m^2/V s, respectively. Optical lithography and successive wet chemical etching are used to define a narrow stripe of the 2DEG. Ohmic contacts are provided by evaporating Ni/AuGe/Au layers and successive thermal annealing. Two metallic gate electrodes, running parallel to the 2DEG stripe, are defined by electron beam lithography and consist of a 50 nm thick Au layer. A schematic picture of the resulting device (sample A) is shown in Fig. 1(a). The 2DEG stripe has a length of 600 μm and a width of 50 μm, while the length of the two metallic gate electrodes is 500 μm with a separation of 1 μm. Different gate voltages U_{g1} and U_{g2} can be applied to the two gates, resulting in two stripes of different carrier density in the electron channel [see Fig. 1(b)]. The gap region between the gates equals the width of the transition region between areas of different carrier densities and will therefore be neglected in the following. The current is applied between the source and the drain contacts at the ends of the 2DEG stripe. The transverse voltage U_y^{exp} is measured by two voltage probes located on each side of the stripe. The measurements are performed in the push-pull configuration,[6] i.e., half of the source-drain voltage U_{sd} is applied at the source and the other half at the drain terminal. The outcome is a symmetric configuration with respect to the voltage probes. The reference sample B is used to determine the relevant sample parameters for the diffusion thermopower model through resistivity, Hall, and Shubnikov–de Haas measurements. In contrast to sample A, sample B has only one gate covering the whole stripe and three voltage probes on each side. If not stated otherwise, all measurements are performed on sample A at 4.2 K.

 ©2012 American Physical Society

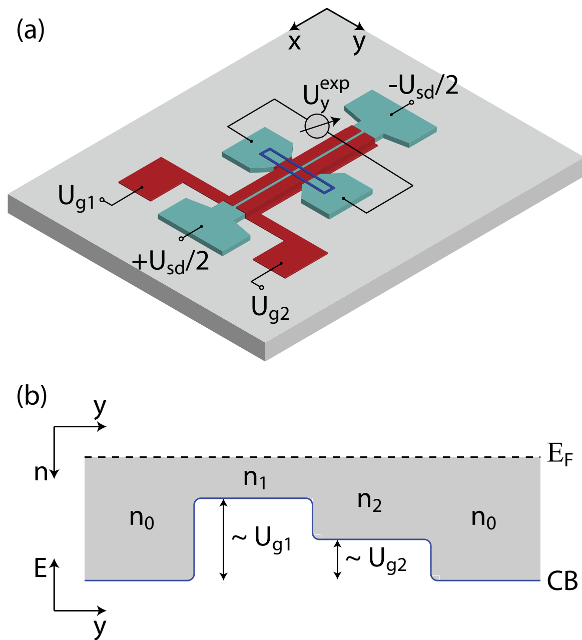

FIG. 1. (Color online) (a) Schematic picture of the rectifier and the experimental setup. The rectifier is measured in the push-pull configuration, i.e., half of the source-drain voltage U_{sd} is applied at one terminal and the other half is applied at the second terminal. The source-drain voltages and the gate voltages U_{g1} and U_{g2} are both referenced to the ground potential. The transverse voltage U_y^{exp} is measured between the left and right voltage probe. The 2DEG defined by an etched mesa is indicated in blue, the metallic gate electrodes in red. The carrier density in the area marked by the blue rectangle is sketched in (b) for $U_{g1} < U_{g2} < 0$ V, which gives a ratchet-type potential landscape. Here, E_F marks the Fermi energy and CB denotes the conduction band (dark-blue curve).

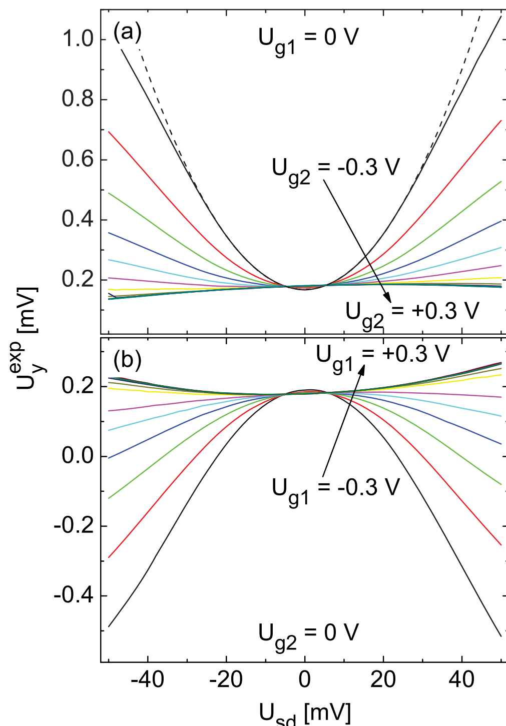

FIG. 2. (Color online) (a) Dependence of the transverse voltage U_y^{exp} on the source-drain voltage U_{sd}. The gate voltage U_{g2} is applied from -0.3 V (black trace) to $+0.3$ V (dark green trace) in steps of 0.05 V, while gate 1 remains grounded ($U_{g1} = 0$ V). The yellow trace shows the transverse voltage for $U_{g2} = 0$ V. The dashed, black line is an exemplary parabolic fit for $U_{sd} \leqslant 25$ mV. (b) Transverse voltage U_y^{exp}, when the role of the gates is switched, i.e., the gate voltage U_{g1} is varied, while gate 2 remains grounded.

III. MEASUREMENTS

Figure 2(a) shows the transverse voltage U_y^{exp} as a function of the source-drain voltage U_{sd}. The gate voltage U_{g2} is varied from -0.3 to 0.3 V in steps of 0.05 V, while the second gate remains grounded ($U_{g1} = 0$ V). The transverse voltage exhibits an almost parabolic dependence on the source-drain voltage, demonstrating transverse rectification in the device. For a gate voltage of $U_{g2} = -0.3$ V, e.g., we find transverse voltages $U_y^{exp} = 1.04$ and 1.07 mV for $U_{sd} = -50$ and 50 mV, respectively. We attribute this negligible deviation from the symmetry relation $U_y^{exp}(U_{sd}) = U_y^{exp}(-U_{sd})$ to small imperfections of the device geometry such as slightly shifted voltage probes and a minute misalignment between the gates and the etched channel. Figure 2(a) also shows that the transverse voltage exhibits a strong dependence on the gate voltage U_{g2}, which will be discussed later in detail. In Fig. 2(b), the role of the gates is switched, i.e., U_{g1} is varied while U_{g2} remains constant. The polarity of the transverse voltage U_y^{exp} has changed, since the direction of the density difference in the electron channel is reversed. In both cases, the polarity of the transverse voltage U_y^{exp} corresponds to an induced flow of electrons from the high-carrier-density area to the low-density area.

To better quantify how the rectification depends on different parameters, we introduce the rectification efficiency. It is defined as the prefactor a_U^{exp} in a parabolic fit to the experimental data $U_y^{exp} = a_U^{exp} U_{sd}^2$ for a bias range $U_{sd} \leqslant 25$ mV (dashed line in Fig. 2). The rectification efficiency is determined for a wide range of gate voltage combinations, and the results are presented in Fig. 3.

Figure 3(a) shows a_U^{exp} as a function of U_{g2} for $U_{g1} = 0$ V. As already observed in Fig. 2, maximum rectification efficiency is seen around $U_{g2} = -0.3$ V, i.e., close to the depletion voltage of the sample. With increasing U_{g2}, a_U^{exp} decreases strongly at first and switches polarity at approximately $U_{g2} = 0$ V. For small positive gate voltages, $|a_U^{exp}|$ increases slowly and saturates for high positive gate voltages ($U_{g2} > 0.1$ V).

The contour plot in Fig. 3(b) gives an overview over a_U^{exp} in the complete range of investigated gate voltages U_{g1} and U_{g2}. It can be seen that the rectification efficiency is antisymmetric, when U_{g1} and U_{g2} are exchanged, and, therefore, vanishes when $U_{g1} = U_{g2}$ (black dashed line). The maximum of $|a_U^{exp}|$ (≈ 0.4 V^{-1}) is observed at roughly $U_{g1} = 0$ V and $U_{g2} = -0.3$ V or vice versa. This can be seen more clearly in Figs. 3(a) and 3(c), which show sections through the data along the $U_{g1} = 0$ V and the $U_{g1} = -0.3$ V line, respectively. The small difference between $|a_U^{exp}(0\,\mathrm{V}, -0.3\,\mathrm{V})|$ and $|a_U^{exp}(-0.3\,\mathrm{V}, 0\,\mathrm{V})|$ is again attributed to imperfections in the fabrication of the sample.

The rectification efficiency in Fig. 3(c) exhibits a nonmonotonic dependence on the gate voltage U_{g2}. This is unexpected

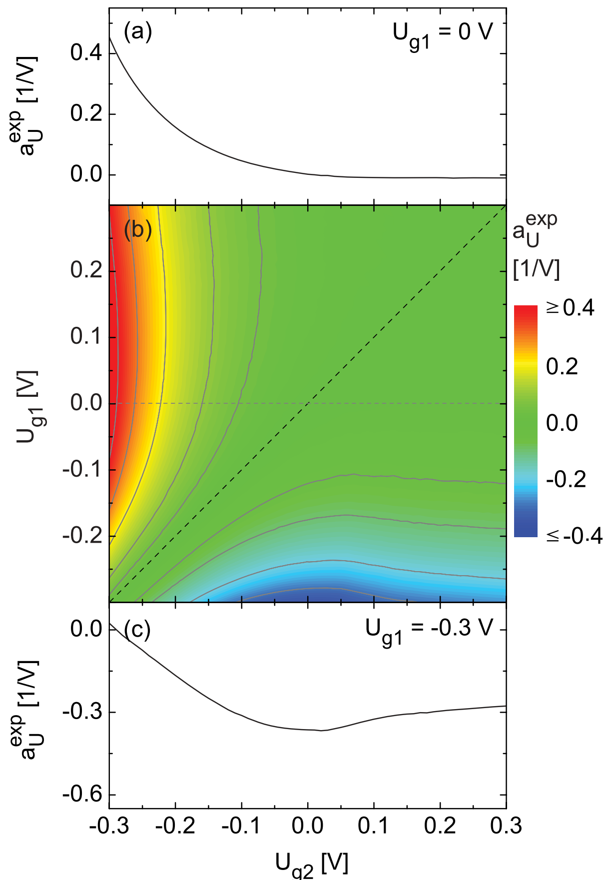

FIG. 3. (Color online) (a) Rectification efficiency a_U^{exp} as a function of U_{g2} for $U_{\mathrm{g1}} = 0$ V, where a_U^{exp} is the coefficient of an $a_U^{\mathrm{exp}} U_{\mathrm{sd}}^2$ fit on the traces shown in Fig. 2 for U_{sd} smaller than 25 mV. (b) Contour plot of the rectification efficiency a_U^{exp} as a function of U_{g1} and U_{g2}. The black dashed line represents $U_{\mathrm{g1}} = U_{\mathrm{g2}}$ and the gray dashed line shows the cross section, which is plotted in (a). The distance between the contour lines is 0.10 V^{-1} with additional contour lines at ± 0.05 V^{-1}. (c) a_U^{exp} in dependence on U_{g2} for $U_{\mathrm{g1}} = -0.3$ V. This trace matches the cross section of the contour plot in (b) at $U_{\mathrm{g1}} = -0.3$ V.

at first, because the carrier density difference increases monotonically with U_{g2}. The fact that $|a_U^{\mathrm{exp}}|$ *decreases* while the density step height increases in the bias range $U_{\mathrm{g2}} > 0$ is an indication that a purely ballistic picture cannot explain the observed rectification. The ballistic deflection of electrons in density-modulated systems[16–19] increases monotonically with increasing step height. So, even though a simple ballistic model may be able to account for some qualitative features of our experiment,[20] a more in-depth treatment is necessary.

Additional insight into the rectification mechanism comes from its temperature dependence. In Fig. 4, the temperature dependences of the rectification efficiency a_U^{exp} (left axis) and carrier mobility μ_0 (right axis, measured on sample B) are presented. The black, red, and green traces show a_U^{exp} in the range from 2 to 30 K for the gate voltages $U_{\mathrm{g2}} = -0.3, -0.2$, and -0.1 V, respectively, while $U_{\mathrm{g1}} = 0$ V. The blue trace shows the temperature dependence of the mobility μ, which was determined using Hall and resistivity measurements. While the mobility decreases roughly linearly, the rectification

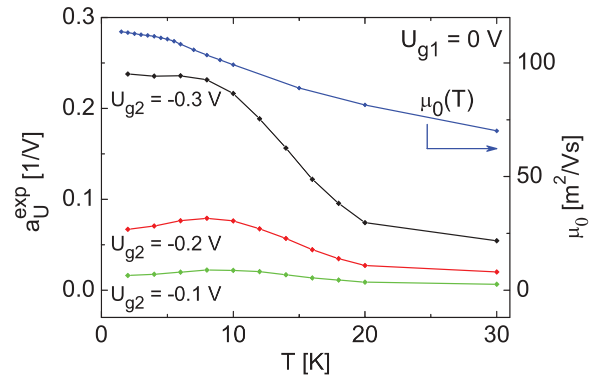

FIG. 4. (Color online) Temperature dependence of the rectification efficiency a_U^{exp} (left axis). The black, red, and green traces show a_U^{exp} as a function of the temperature T for $U_{\mathrm{g2}} = -0.3, -0.2$, and -0.1 V, respectively. The blue trace shows the temperature dependence of the mobility μ measured on the reference sample B (right axis).

efficiency shows a more complex behavior, in particular for $U_{\mathrm{g2}} = -0.2$ and -0.1 V, where a_U^{exp} exhibits a maximum at approximately 8–10 K. This again indicates that the observed rectification is not a purely ballistic effect, which would directly reflect the electron mobility or, equivalently, the elastic mean free path.

IV. DIFFUSION THERMOPOWER MODEL

In the following, we show that the measured transverse voltage U_y^{exp} can be explained within a diffusion thermopower model. The relevant part of the rectifier is shown schematically in Fig. 5. We distinguish different regions; the electron channel, through which a finite current is driven, consists of two stripes 1 and 2 with, in general, different carrier concentrations n_1 and n_2. The voltage probes are current-free and remain at

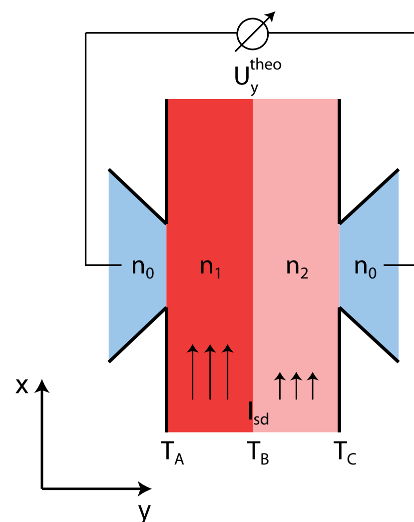

FIG. 5. (Color online) Schematic sketch of the rectifier. The system is divided into four regions: the two stripes of the electron channel plus the two voltage probes. The current-free voltage probes have carrier density n_0; the two stripes have (tunable) carrier concentrations n_1 and n_2.

carrier concentration n_0, independent of the gate voltages. The current along the electron channel increases the local electron temperature from the lattice temperature T_0 to $T = T_0 + \delta T$ via Joule heating. The density modulation in the perpendicular direction of the electron channel introduces both a y dependence of the temperature $T(y)$ (via the carrier-density dependence of the resistivity) and of the Seebeck coefficient $S(y)$, which characterizes the strength of the thermopower. This results in a finite thermoelectric voltage

$$U_y^{\mathrm{theo}} = \int_{-\infty}^{\infty} dy\, S(y)\, \partial_y T(y), \tag{1}$$

between the contacts of the voltage probes that are far outside the heated region, $T(\infty) = T(-\infty) = T_0$. Neglecting the y dependence of the Seebeck coefficient in Eq. (1) would lead to an exact cancellation of the contributions from regions with positive and negative temperature gradients. However, when taking the y dependence of S into account, the region with the smaller carrier concentration dominates (since it has a larger Seebeck coefficient), and the thermoelectric voltage, Eq. (1), is nonvanishing.

For a quantitative analysis, we employ a semiclassical transport theory.[21] The y components of the electric and the heat current densities, j_y and j_y^q, respectively, are related to the gradients of the electrochemical potential ϕ and temperature T via

$$\begin{pmatrix} j_y \\ j_y^q \end{pmatrix} = -\begin{pmatrix} L_{11} & L_{12} \\ L_{21} & L_{22} \end{pmatrix} \begin{pmatrix} \partial_y \phi \\ \partial_y T \end{pmatrix}. \tag{2}$$

The coefficients L_{ij} are related to the electric conductivity σ, the Seebeck coefficient S, and the thermal conductivity κ via $L_{11} = \sigma$, $S = L_{12}/L_{11}$, $L_{21} = T L_{12}$, and $\kappa = L_{22} - L_{12}L_{21}/L_{11}$.

The electron temperature profile is determined by the continuity equation for the heat current,

$$\nabla \cdot \mathbf{j}^q = \mathbf{j} \cdot \mathbf{E} - c_V \frac{T - T_0}{\tau_{\mathrm{i}}}. \tag{3}$$

The first (source) and second (drain) term on the right-hand side account for Joule heating and heat transfer to the lattice, respectively. The latter is modeled by a relaxation term, linearized in $T - T_0$, that includes the specific-heat capacity c_V, the difference between the electron (T) and lattice (T_0) temperature, and a heat relaxation time $\tau_{\mathrm{i}}(\epsilon)$ taken at the Fermi energy, $\tau_{\mathrm{i}} = \tau_{\mathrm{i}}(\epsilon_F)$. We remark here that the relaxation time τ_{i} for the heat transfer to the lattice differs from the relaxation time τ entering the electric conductivity. For τ_{i}, only those electron scattering processes that are accompanied by an energy change larger than $k_B T$ are relevant (dubbed as *inelastic* scattering in contrast to *elastic* scattering, for which the energy transfer is much smaller than $k_B T$).[22] In contrast, both elastic and inelastic scattering processes contribute to the (energy-dependent[23,24]) relaxation time entering the electric conductivity, $\tau^{-1}(\epsilon) = \tau_{\mathrm{e}}^{-1}(\epsilon) + \tau_{\mathrm{i}}^{-1}(\epsilon)$. In the system described here, elastic scattering strongly dominates, $\tau_{\mathrm{e}} \ll \tau_{\mathrm{i}}$, and we can set $\tau \approx \tau_{\mathrm{e}}$.

Since the charge current density has only an x component, which does not depend on the position x, we simplify Eq. (3) by using $\nabla \cdot \mathbf{j}^q = \partial_y j_y$ and $\mathbf{j} \cdot \mathbf{E} = \sigma E_x^2$ and combine it with the definition of the thermal conductivity, $j_y^q = -\kappa\, \partial_y T$, to obtain a differential equation

$$T - l^2 \partial_y^2 T = \frac{(eE_x l)^2}{\kappa/\sigma} + T_0. \tag{4}$$

This equation describes the variation of the temperature on the scale given by the energy diffusion length $l = \sqrt{\kappa \tau_{\mathrm{i}}/c_V}$, which is considerably larger than the mean free path in the 2DEG.

Calculating σ, κ, and c_V to lowest order in the Sommerfeld expansion (valid for $k_B T \ll \epsilon_F$) yields the energy diffusion length

$$l = v_F \sqrt{\frac{\tau_{\mathrm{i}} \tau_{\mathrm{e}}}{2}}, \tag{5}$$

with $\tau_{\mathrm{e}} = \tau_{\mathrm{e}}(\epsilon_F)$, and the Wiedemann-Franz law $\kappa/\sigma = (\pi k_B/e)^2 T/3$. We use $v_F = \sqrt{2\epsilon_F/m^*}$, where m^* is the effective electron mass in GaAs. Furthermore, the Fermi energy ϵ_F (relative to the lower subband edge) is related to the two-dimensional density n of the electron gas via $\epsilon_F = n\pi\hbar^2/m^*$. This expression also relates the carrier density to the gate voltages U_{g1} and U_{g2} via $\epsilon_F/\epsilon_0 = 1 + U_{\mathrm{g}i}/U_{\mathrm{g}}^{\mathrm{dep}}$, where ϵ_0 is the Fermi energy at zero gate voltage and $U_{\mathrm{g}}^{\mathrm{dep}} = -0.38$ V is the depletion voltage.

Applying the Sommerfeld expansion, the Seebeck coefficient S can be expressed in terms of the electric conductivity by the Mott formula[21,25]

$$S = -\frac{\pi^2}{3} \frac{k_B^2 T}{e} \frac{\sigma'}{\sigma}, \tag{6}$$

with $\sigma = \sigma(\epsilon_F)$ and $\sigma' = \partial_\epsilon \sigma(\epsilon)|_{\epsilon_F}$, where (for a two-dimensional electron gas) $\sigma(\epsilon) = e^2 \epsilon \tau_{\mathrm{e}}(\epsilon)/(\pi\hbar^2)$.

For a systematic perturbation expansion up to second order in E_x, we replace T by T_0 in the ratio κ/σ and in the Mott formula, Eq. (6). Then, the solution of Eq. (4) is given by

$$T_i(y) = T_i^{\mathrm{bulk}} + T_i^- e^{-y/l_i} + T_i^+ e^{y/l_i} \tag{7}$$

for each region i of constant carrier density. The asymptotic bulk value T_i^{bulk} is reached far away from the steps: $T_0^{\mathrm{bulk}} = T_0$ deep in the voltage probes and $T_i^{\mathrm{bulk}} = T_0 + (eE_x l_i)^2/(\frac{\pi^2}{3} k_B^2 T_0)$ with the corresponding energy diffusion length l_i for the two stripes $i = 1$ and 2 in the electron channel, respectively.

The constants $T_i^{\pm}$ for each stripe are determined by the boundary conditions. To fully determine all constants, we need two conditions for each interface between regions of different carrier concentration. One is readily obtained by requiring that the heat current $j_y^q = -\kappa \partial_y T$ entering an interface from one side equals the one leaving from the other side, which has the consequence for the system under study that the product $n\tau_{\mathrm{e}}\partial_y T$ is continuous at each interface. As a second condition, we find that, for $\tau_{\mathrm{i}} \gg \tau_{\mathrm{e}}$, the temperature itself is continuous.[26]

To calculate the thermoelectric voltage, it is necessary to determine the (energy-dependent) relaxation rates $\tau_{\mathrm{e}}(\epsilon)$ and $\tau_{\mathrm{i}}(\epsilon)$. A theoretical estimate of these relaxation rates would depend on various model assumptions and, thus, introduce uncertainties that make a quantitative comparison with experiment difficult. Therefore, we determine them experimentally by performing (gate-voltage-dependent) resistivity, Hall, and Shubnikov–de Haas measurements on reference sample B.

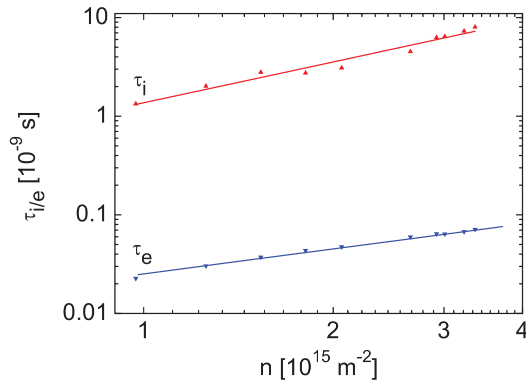

FIG. 6. (Color online) Energy dependence of the elastic scattering time τ_e (blue) and the inelastic scattering time τ_i (red). The first data points match $U_{g2} = -0.2$ V and the gate voltage increases by 0.05 V for each data point. The lines correspond to the linear fits of the data.

The inelastic relaxation time τ_i is determined from the relation between electron temperature T and source-drain current I_{sd} in the heat balance equation (3), after we set $\nabla \cdot \mathbf{j}^q = \mathbf{0}$.[27] The latter is justified since, for all x positions at which there is no voltage probe, the temperature and, thus, the heat current are independent of y for sample B. To measure $T(I_{sd})$, we use the temperature dependence of the Shubnikov–de Haas (SdH) oscillations of two-dimensional electrons under low magnetic fields.[28–30] This is done by first measuring the SdH oscillations at different lattice temperatures T_0 with a small current I_{sd} of 100 nA, such that the electron temperature T equals the lattice temperature. Then, the SdH oscillations are measured at a fixed lattice temperature T_0 with different heating currents I_{sd}. The comparison of the SdH-oscillation amplitudes in the two different schemes yields $T(I_{sd})$. An alternative approach to determine $T(I_{sd})$ would be to measure the temperature-dependent resistivity.[31] Using SdH oscillations, however, has the advantage that its amplitude depends only on the electron but not the lattice temperature, in contrast to the resistivity, which, in general, depends on both the electron and the lattice temperature.

The results for $\tau_e(\epsilon)$ and $\tau_i(\epsilon)$ are shown in Fig. 6. Fitting a power-law function, $\tau_e = \tau_{e,0}(\epsilon/\epsilon_0)^{\alpha_e}$ and $\tau_i = \tau_{i,0}(\epsilon/\epsilon_0)^{\alpha_i}$ yields $\tau_{e,0} = 4.7 \times 10^{-11}$ s and $\tau_{i,0} = 3.7 \times 10^{-9}$ s, and for the exponents, $\alpha_e = 0.88 \pm 0.04$ and $\alpha_i = 1.45 \pm 0.09$, which is in good agreement with theoretical predictions.[32]

Having determined $\tau_e(\epsilon)$ and $\tau_i(\epsilon)$, we calculate the temperature profile, see Fig. 7, across the sample at the position where the voltage probes are attached. If the energy diffusion lengths l_i were much smaller than the transport-channel widths, then the temperature profile would be a step function (dashed curves in Fig. 7) with $T_i = T_i^{\text{bulk}}$ (gray area in Fig. 7). In our sample, however, the channel width is of the same order of magnitude as l_i (for $U_{gi} = -0.2$ V/0 V/+0.2 V, the energy diffusion length is $l_i = 16.8$ μm/58.2 μm/117.7 μm). As a consequence, we find a strong y dependence of the temperature (solid lines in Fig. 7), which does not approach the asymptotic bulk values T_i^{bulk} in the two stripes of the electron channel. Changing the gate voltage U_{g2} in stripe 2 changes the energy diffusion length l_2 there and, thus, T_2^{bulk}. However, it also affects T_1^{bulk} since for fixed I_{sd} the electric field E_x changes when the carrier density and, thus, the overall resistance are modified. As the temperature varies on the length scale of l_i, the gap between the gates, which is much smaller than l_i, can be neglected, as mentioned previously.

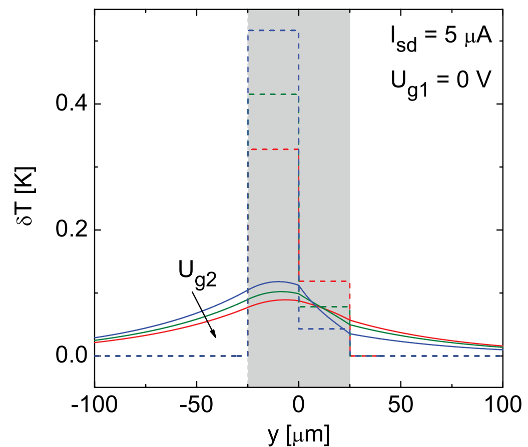

FIG. 7. (Color online) Heating correction to the temperature of the electron system for $I_{sd} = 5$ μA, $U_{g1} = 0$ V, and three different values for U_{g2}: $U_{g2} = -0.2$ V (blue), $U_{g2} = -0.15$ V (green), and $U_{g2} = -0.1$ V (red). The horizontal dashed lines are the heating temperatures for channels with infinite width for the gate voltage U_{g2} of corresponding color. The gray region shows the electron transport channel and the vertical dashed lines separate the two stripes with different carrier density from the voltage probes left and right of the channel.

V. THEORETICAL RESULTS AND DISCUSSION

Finally, we plug the temperature profile into Eq. (1) to obtain the thermoelectric voltage. To translate the experimentally applied source-drain voltage U_{sd} into the electric field E_x entering the theory, we take an (experimentally estimated) value of $R_0 = 450\ \Omega$ for the contact resistances from the source and drain contacts. The result of our simulation for the same parameters as in Fig. 3 is shown in Fig. 8. We find a very good agreement between a_U^{exp} and a_U^{theo} as a function of the gate voltages U_{g1} and U_{g2}. In particular, we reproduce the nonmonotonic dependence of the rectification efficiency on the density modulation; see Fig. 8(c). (Note that the exact position of the calculated maximum depends on the contact resistance R_0.)

The nonmonotonic behavior of $a_U(U_{g1},U_{g2})$ can be explained intuitively within the framework of the diffusion thermopower model by two contrary dependencies. On the one hand, no rectification can be observed for symmetrically biased gates $U_{g2} = U_{g1} = -0.3$ V so that the efficiency starts from zero (at $U_{g2} = -0.3$ V) and increases as the gate voltage is increased. On the other hand, the thermoelectric effect decreases with increasing carrier density as the resistivity and, correspondingly, the Joule heating decreases. This eventually leads to a decrease of the overall effect, as observed in the range $U_{g2} > 0.1$ V.

For a quantitative comparison between theory and experiment, we want to avoid the uncertainty associated with the estimate of the contact resistance R_0. To this end, we repeat the measurement of the transverse voltage but relate it to the applied current I_{sd} rather than the voltage U_{sd}. This defines

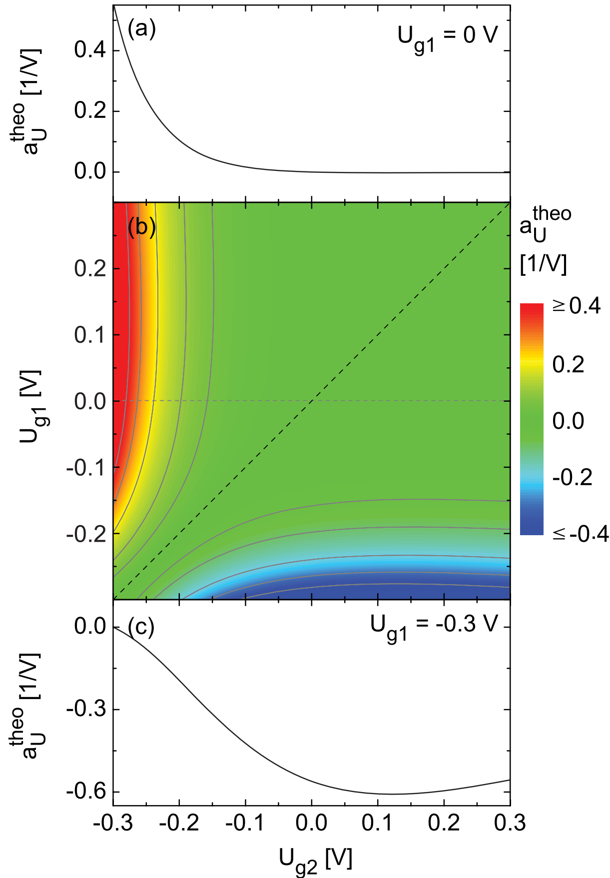

FIG. 8. (Color online) (a) Calculated rectification efficiency a_U^{theo} as a function of U_{g2} for $U_{\text{g1}} = 0$ V. (b) Contour plot of the calculated rectification efficiency a_U^{theo} as a function of U_{g1} and U_{g2}. The distance between the contour lines is 0.1 V^{-1} with additional contour lines at ± 0.05 V^{-1}. (c) a_U^{theo} in dependence on U_{g2} for $U_{\text{g1}} = -0.3$ V. This trace matches the cross section of the contour plot in (b) at $U_{\text{g1}} = -0.3$ V.

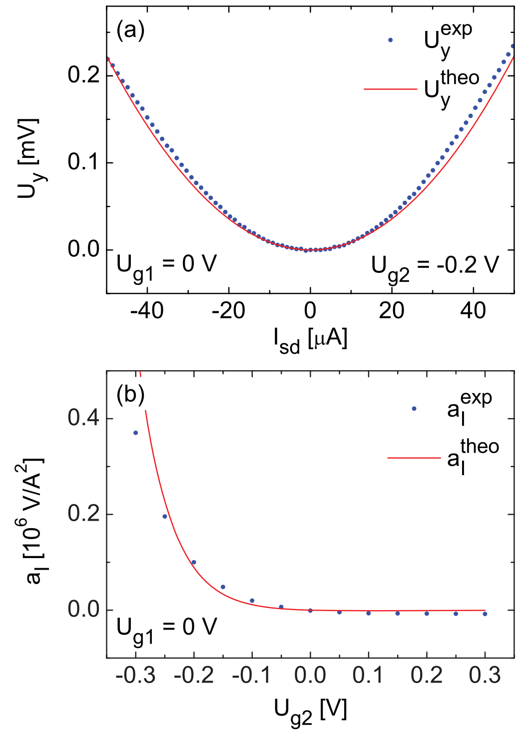

FIG. 9. (Color online) Comparison between the measured and the calculated rectification effect: (a) Dependence of the measured transverse voltage U_y^{exp} (blue dots) and the calculated transverse voltage U_y^{theo} (red trace) on the heating current I_{sd} for $U_{\text{g1}} = 0$ V and $U_{\text{g2}} = -0.2$ V. (b) Dependence of the measured rectification efficiency a_U^{exp} (blue dots) and the calculated rectification efficiency a_U^{theo} (red trace) on U_{g2}.

the rectification efficiency $a_I = U_y / I_{\text{sd}}^2$. Figure 9 shows a comparison between the experimental and the calculated data. In Fig. 9(a), the transverse voltage U_y^{exp} (blue dots) and the calculated thermoelectric voltage U_y^{theo} (red trace) are plotted as a function of I_{sd} for $U_{\text{g1}} = 0$ V and $U_{\text{g2}} = -0.2$ V. We find that U_y^{theo} shows the same parabolic dependence on I_{sd} as U_y^{exp}. A comparison of the measured, a_I^{exp}, and calculated, a_I^{theo}, rectification efficiency as a function of gate voltage is presented in Fig. 9(b). It should be pointed out that no adjustable parameters have been used in the calculation, since all relevant parameters were independently determined on the homogeneous reference sample B. The small quantitative deviation can be explained by the approximations that were made both in the experimental evaluation and in the theoretical treatment. Also, phonon effects, such as phonon drag, which can play a role in AlGaAs heterostructures,[33–36] have been neglected here.

In view of the diffusion thermopower model, it is now also possible to better understand why the rectification efficiency a_U^{exp} and the mobility μ_0 exhibit such different temperature dependencies (see Fig. 4). Both quantities are affected by τ_{i}, which has a $1/T$ dependence on the temperature,[37] and τ_{e}, which is almost constant in the temperature range of interest. The relaxation time τ that determines the mobility μ_0 is given by Matthiessen's rule $\tau^{-1}(\epsilon) = \tau_{\text{e}}^{-1}(\epsilon) + \tau_{\text{i}}^{-1}(\epsilon)$, and because $\tau_{\text{e}} \ll \tau_{\text{i}}$, the temperature dependence of τ_{i} will only slightly affect the overall mobility. The energy diffusion length, on the other hand, is proportional to $\sqrt{\tau_{\text{i}}\tau_{\text{e}}}$ [see Eq. (5)], so that the temperature dependence of τ_{i} will affect the rectification efficiency considerably, regardless of how small τ_{e} is compared to τ_{i}. The slight increase of a_U^{exp} at low temperatures may be attributed to an effective increase of τ_{i} due to the fact that only scattering processes in which the transferred energy is larger than $k_B T$ contribute to τ_{i}, i.e, with increasing T, fewer processes contribute.

The experiment and its explanation within the diffusion thermopower model have a number of interesting consequences. Because of the nonmonotonic $a_U(U_{\text{g1}}, U_{\text{g2}})$ dependence, the rectification is not "transitive," i.e., $a_U(U_A, U_B) + a_U(U_B, U_C) \neq a_U(U_A, U_C)$. Therefore, in samples with multiple stripes, the rectification can be cascaded to improve the output voltage. If such a sample is periodic, e.g., with three sets of stripes $\ldots ABCABCABC \ldots$, it would constitute a ratchet-type potential (see, e.g., Olbrich *et al.*[38] and references therein), where an agitation along the stripes would induce a current/voltage *perpendicular* to the driving signal. Our present setup with a carrier density profile $ABCA$ [voltage probe – first stripe – second stripe – voltage probe; see also Fig. 1(b)] constitutes the smallest unit of such a transverse ratchet.

Going back to the introductory remarks, our work also bridges the two concepts for rectification, i.e., change of material versus noncentrosymmetric guidance of electrons. The two parallel stripes can be considered as two different (but tunable!) materials, which have been interfaced to induce rectification that does not rely on ballistic effects but rather on diffusion thermopower. Nevertheless, we do observe finite-size effects. This is a feature that necessarily appears in ballistic rectifiers as well, although with a different characteristic length. While the width of our sample is much larger than the elastic mean free path (the characteristic length for ballistic transport), it is smaller than the energy diffusion length l. This leads to a strong reduction of the temperature difference (see Fig. 7) and, therefore, the rectification efficiency.

VI. SUMMARY

In conclusion, we have demonstrated tunable rectification in a density-modulated two-dimensional system. The polarity and value of the rectified transverse voltage depend on the direction and magnitude of the density modulation of the carrier densities inside the electron channel. We show that the observed data are in good qualitative and quantitative agreement with a diffusion thermopower model. Our findings have a number of consequences for the understanding of so-called ballistic rectifiers and related structures.

ACKNOWLEDGMENTS

We acknowledge stimulating discussions with Daniel Urban and financial support from DFG via SPP 1285.

[1] A. M. Song, A. Lorke, A. Kriele, J. P. Kotthaus, W. Wegscheider, and M. Bichler, Phys. Rev. Lett. **80**, 3831 (1998).

[2] K. Hieke and M. Ulfward, Phys. Rev. B **62**, 16727 (2000).

[3] I. Shorubalko, H. Q. Xu, I. Maximov, P. Omling, L. Samuelson, and W. Seifert, Appl. Phys. Lett. **79**, 1384 (2001).

[4] L. Worschech, H. Q. Xu, A. Forchel, and L. Samuelson, Appl. Phys. Lett. **79**, 3287 (2001).

[5] B. Hackens, L. Gence, C. Gustin, X. Wallart, S. Bollaert, A. Cappy, and V. Bayot, Appl. Phys. Lett. **85**, 4508 (2004).

[6] M. Knop, U. Wieser, and U. Kunze, Appl. Phys. Lett. **88**, 082110 (2006).

[7] S. Sassine, Y. Krupko, J. C. Portal, Z. D. Kvon, R. Murali, K. P. Martin, G. Hill, and A. D. Wieck, Phys. Rev. B **78**, 045431 (2008).

[8] A. M. Song, P. Omling, L. Samuelson, W. Seifert, I. Shorubalko, and H. Zirath, Appl. Phys. Lett. **79**, 1357 (2001).

[9] D. Spanheimer, C. R. Müller, J. Heinrich, S. Höfling, L. Worschech, and A. Forchel, Appl. Phys. Lett. **95**, 103502 (2009).

[10] A. Lorke, S. Wimmer, B. Jager, J. P. Kotthaus, W. Wegscheider, and M. Bichler, Physica B **249**, 312 (1998).

[11] I. Shorubalko, H. Q. Xu, I. Maximov, D. Nilsson, P. Omling, L. Samuelson, and W. Seifert, Electron. Dev. Lett. **23**, 377 (2002).

[12] R. Fleischmann and T. Geisel, Phys. Rev. Lett. **89**, 016804 (2002).

[13] S. de Haan, A. Lorke, J. P. Kotthaus, M. Bichler, and W. Wegscheider, Physica E **21**, 916 (2004).

[14] D. Salloch, U. Wieser, U. Kunze, and T. Hackbarth, Appl. Phys. Lett. **94**, 203503 (2009).

[15] M. Wiemann, U. Wieser, U. Kunze, D. Reuter, and A. D. Wieck, Appl. Phys. Lett. **97**, 062112 (2010).

[16] J. Spector, H. L. Stormer, K. W. Baldwin, L. N. Pfeiffer, and K. W. West, Appl. Phys. Lett. **56**, 1290 (1990).

[17] J. Spector, H. L. Stormer, K. W. Baldwin, L. N. Pfeiffer, and K. W. West, Appl. Phys. Lett. **56**, 2433 (1990).

[18] M. Noguchi, H. Sakakibara, and T. Ikoma, Jpn. J. Appl. Phys. **32**, 5014 (1993).

[19] Y. K. Fukai, S. Tarucha, Y. Hirayama, Y. Tokura, and T. Saku, Appl. Phys. Lett. **60**, 106 (1992).

[20] A. Ganczarczyk, C. Notthoff, M. Geller, A. Lorke, D. Reuter, and A. D. Wieck, in *Physics of Semiconductors: 29th International Conference on the Physics of Semiconductors*, AIP Conference Proceedings No. 1199, edited by Marília Caldas and Nelson Studart (AIP, New York, 2009), p. 143.

[21] N. W. Ashcroft and N. D. Mermin, *Solid State Physics* (Saunders College, Philadelphia, 1976).

[22] T. Kawamura and S. Das Sarma, Phys. Rev. B **45**, 3612 (1992).

[23] W. Walukiewicz, H. E. Ruda, J. Lagowski, and H. C. Gatos, Phys. Rev. B **30**, 4571 (1984).

[24] J. J. Harris, J. A. Pals, and R. Woltjer, Rep. Prog. Phys. **52**, 1217 (1989).

[25] M. Cutler and N. F. Mott, Phys. Rev. **181**, 1336 (1969).

[26] This is proven by writing the electric and the heat current through each interface as functions of the steps in temperature, ΔT, and electrochemical potential, $\Delta\phi$, and linearizing in ΔT and $\Delta\phi$. The resulting expressions depend on the transmission properties at the interface but are independent of τ_i and τ_e. The requirement of a vanishing electric current relates ΔT to $\Delta\phi$ in a linear way, i.e., the heat current is also a linear function of ΔT. This heat current has to match the heat current $j_y^q = -\kappa\partial_y T$ entering the interface, which scales with the amplitude of the temperature increase δT times $\kappa/l \propto \sqrt{\tau_e/\tau_i}$. Therefore, ΔT scales with $\sqrt{\tau_e/\tau_i}$ times the amplitude of δT and can, as a consequence, be neglected in the limit $\tau_i \gg \tau_e$. This also justifies Eq. (6), which determines the thermopower everywhere away from the interfaces only, with no extra contributions from the interfaces.

[27] L. W. Molenkamp, H. van Houten, C. W. J. Beenakker, R. Eppenga, and C. T. Foxon, Phys. Rev. Lett. **65**, 1052 (1990).

[28] K. von Klitzing, G. Dorda, and M. Pepper, Phys. Rev. Lett. **45**, 494 (1980).

[29] T. Ando, A. B. Fowler, and F. Stern, Rev. Mod. Phys. **54**, 437 (1982).

[30] K. Hirakawa and H. Sakaki, Appl. Phys. Lett. **49**, 889 (1986).

[31] S. J. Manion, M. Artaki, M. A. Emanuel, J. J. Coleman, and K. Hess, Phys. Rev. B **35**, 9203 (1987).

[32] E. H. Hwang and S. Das Sarma, Phys. Rev. B **77**, 235437 (2008).

[33] R. Fletcher, J. C. Maan, K. Ploog, and G. Weimann, Phys. Rev. B **33**, 7122 (1986).

[34] R. Fletcher, M. D'Iorio, A. S. Sachrajda, R. Stoner, C. T. Foxon, and J. J. Harris, Phys. Rev. B **37**, 3137 (1988).

[35] C. Ruf, H. Obloh, B. Junge, E. Gmelin, K. Ploog, and G. Weimann, Phys. Rev. B **37**, 6377 (1988).

[36] W. E. Chickering, J. P. Eisenstein, and J. L. Reno, Phys. Rev. Lett. **103**, 046807 (2009).

[37] Y. Okuyama and N. Tokuda, Phys. Rev. B **40**, 9744 (1989).

[38] P. Olbrich, J. Karch, E. L. Ivchenko, J. Kamann, B. März, M. Fehrenbacher, D. Weiss, and S. D. Ganichev, Phys. Rev. B **83**, 165320 (2011).